High-speed laser microsurgery of alert fruit flies for fluorescence imaging of neural activity

Supriyo Sinha[a,b,1], Liang Liang[a,b], Eric T. W. Ho[c], Karel E. Urbanek[b], Liqun Luo[a,d], Thomas M. Baer[b,e,1], and Mark J. Schnitzer[a,b,d,f,1]

Departments of [a]Biology, [b]Applied Physics, and [c]Electrical Engineering, [d]Howard Hughes Medical Institute, [e]Stanford Photonics Research Center, and [f]CNC Program, Stanford University, Stanford, CA 94305

Edited by Ehud Y. Isacoff, University of California, Berkeley, CA, and accepted by the Editorial Board September 5, 2013 (received for review September 24, 2012)

Intravital microscopy is a key means of monitoring cellular function in live organisms, but surgical preparation of a live animal for microscopy often is time-consuming, requires considerable skill, and limits experimental throughput. Here we introduce a spatially precise (<1-μm edge precision), high-speed (<1 s), largely automated, and economical protocol for microsurgical preparation of live animals for optical imaging. Using a 193-nm pulsed excimer laser and the fruit fly as a model, we created observation windows (12- to 350-μm diameters) in the exoskeleton. Through these windows we used two-photon microscopy to image odor-evoked Ca^{2+} signaling in projection neuron dendrites of the antennal lobe and Kenyon cells of the mushroom body. The impact of a laser-cut window on fly health appears to be substantially less than that of conventional manual dissection, for our imaging durations of up to 18 h were ∼5–20 times longer than prior in vivo microscopy studies of hand-dissected flies. This improvement will facilitate studies of numerous questions in neuroscience, such as those regarding neuronal plasticity or learning and memory. As a control, we used phototaxis as an exemplary complex behavior in flies and found that laser microsurgery is sufficiently gentle to leave it intact. To demonstrate that our techniques are applicable to other species, we created microsurgical openings in nematodes, ants, and the mouse cranium. In conjunction with emerging robotic methods for handling and mounting flies or other small organisms, our rapid, precisely controllable, and highly repeatable microsurgical techniques should enable automated, high-throughput preparation of live animals for optical experimentation.

laser surgery | calcium imaging | *Drosophila melanogaster*

Intravital imaging of small model organisms is a staple technique in many fields of biomedicine. Gaining optical access to the body's interior usually requires removal or thinning of a highly scattering, protective exterior. Unfortunately, surgical creation of an optical window is generally time-consuming, requires considerable skill and dexterity, and often represents an unwanted source of experimental variability. To address these challenges, we created laser surgical means to open optical windows in the bodies of live animals.

Our approach is adaptable to many species and applications, but we mainly focused on fluorescence brain imaging in alert fruit flies, a pursuit of growing importance for the study of neural systems (1, 2). Most prior studies that have monitored flies' neural activity have relied on immobilized fly preparations suitable for optical microscopy (3, 4) or electrophysiology (5, 6). Recent improvements in genetically encoded Ca^{2+} indicators and imaging methods now allow in vivo fluorescence imaging of neural activity in behaving flies (2). The fly brain's small size, <250 μm deep in the adult, is conducive to two-photon imaging of a variety of neural populations after opening of the cuticle (2, 4).

Multiple laboratories have developed protocols to prepare flies for imaging of neural activity (2, 7), but the basic steps are similar (Fig. 1*A*). Removal of the cuticle and underlying air sacs is important for imaging because these structures strongly scatter light. The traditional means of removing the cuticle, manual dissection using sharp forceps, is time-consuming, requires considerable skill, and can lead to poor experimental reproducibility. Further, the use of forceps can traumatize the brain, compromising the fly's behavior. These drawbacks motivated our examination of whether laser microsurgery might provide an alternative approach.

To date, several groups have reported microsurgical methods based on ultrashort-pulsed laser amplifiers (8–10). These methods are suited for ablating volumes a few microns or less in diameter, such as single cells (10), or for subsurface ablation (8). To ablate larger tissue volumes, these surgical systems typically require laser-scanning mechanisms. Thus, as the surgical volume increases, the duration of surgery rises proportionally. Further, the size, cost, and operational complexity of ultrashort-pulsed laser amplifiers are all sufficiently great that biologists have not widely adopted this approach. Nor was it an affordable or pragmatic option for our work because we needed an economical system useable in a turnkey fashion by biologists with no hands-on experience in laser alignment or tuning.

Hence, we considered whether UV excimer lasers might enable simpler, faster, and more affordable microsurgical methods for biological research. Due to their substantial photon energies and fluences, nanosecond-pulsed UV lasers have enabled attractive solutions for surgical removal or cutting of tissue in a variety of applications (11, 12). It was previously unexplored

Significance

Microscopy and neurophysiology experiments in live animals commonly involve complex surgical preparations, which are often time-consuming, demand considerable manual dexterity, and can sharply limit experimental throughput. Here we present a spatially precise laser microsurgical technique using a pulsed UV laser. Our approach reduces surgical time by up to two orders of magnitude while substantially improving reproducibility. Using the fruit fly as a model, we show that laser microsurgery leaves complex behaviors intact and allows us to visualize brain activity in live flies for up to 18 h, more than four times longer than reported previously using hand dissection. We also demonstrate laser microsurgery on nematodes, ants, and the mouse cranium, illustrating broad potential utility for both optical and electrophysiological studies.

Author contributions: S.S., L. Luo, T.M.B., and M.J.S. designed research; S.S., L. Liang, E.T.W.H., and K.E.U. performed research; T.M.B. and M.J.S. supervised research; and S.S. and M.J.S. wrote the paper.

The authors declare no conflict of interest.

This article is a PNAS Direct Submission. E.Y.I. is a guest editor invited by the Editorial Board.

[1]To whom correspondence may be addressed. E-mail: mschnitz@stanford.edu, tmbaer@stanford.edu, or supriyo@stanford.edu.

This article contains supporting information online at www.pnas.org/lookup/suppl/doi:10.1073/pnas.1216287110/-/DCSupplemental.

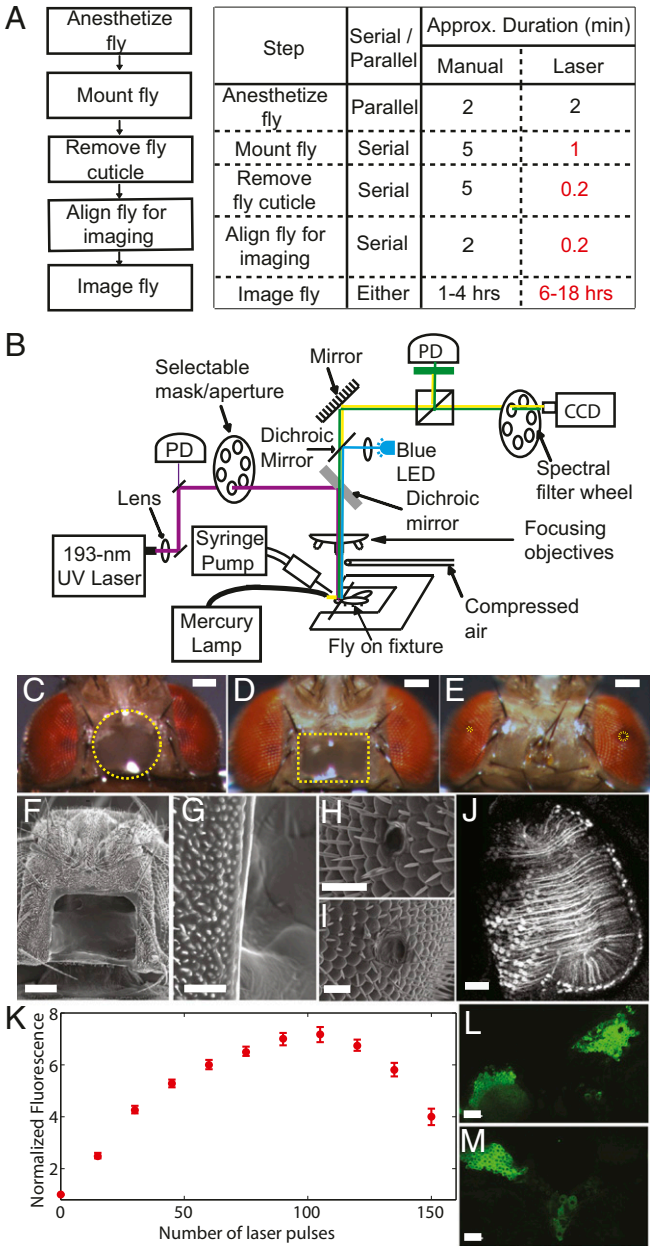

Fig. 1. Laser microsurgery of fruit flies is faster and more precise than manual dissection. (*A*) (*Left*) Work flow for imaging flies in vivo. (*Right*) Approximate durations for each step. Red font indicates steps at which our protocol improves over conventional methods. (*B*) Schematic of the laser microsurgery station based on a 193-nm-wavelength excimer laser. To monitor surgical progress, light from a blue LED enables imaging of green fluorescence from the fly. Photodiodes (PD) provide readouts of laser power and fluorescence emissions. A mercury lamp with gooseneck fiber output enables bright-field imaging. A flow of air prevents ejected debris from the surgery from depositing on the focusing objective. A syringe pump enables immediate application of artificial haemolymph after surgery. All components are computer-controlled, except for the mercury lamp. (*C*–*E*) Bright-field images of flies after laser surgery. Flies with large circular (285-μm-diameter) (*C*), large rectangular (275 μm × 175 μm) (*D*), and small circular (12-μm-diameter, left eye; 25-μm-diameter, right eye) (*E*) windows cut in the cuticle or retina illustrate the user's ability to choose the shape, size, and location of the window via the selectable mask shown in *B*. Dotted yellow lines highlight the incisions. (Scale bar, 100 μm.) (*F*) Scanning electron micrograph (SEM) of a fly with a rectangular window cut in the cuticle. Sharp edges are visible. (Scale bar, 100 μm.) (*G*) Close-up image of one of the cut edges from *F*, highlighting the precision of the cut and its straightness to ~100 nm. (Scale bar, 10 μm.) (*H* and *I*) SEM images of holes cut in the retina of the fly shown in *E*. *H* and *I* show the holes cut in the left and right retinae, respectively. (Scale bar, 25 μm.) (*J*) Two-photon image of *+/CyO;21DhhGal4, UAS-TNXXLH.3*Z3/TM6B* fly following a microsurgery in which 150 pulses (350-μJ pulses; 100 Hz) drilled through the retina of a fly mounted on its side (spot size 400 μm × 350 μm). The image is a maximum-intensity projection of a 3D image stack (143 slices acquired at 1-μm intervals). (Scale bar, 25 μm.) (*K*) Signal intensity from fluorescently labeled neurons lying under the cuticle rises with the number of laser pulses used (200 μJ each) to drill a 300-μm-diameter circular spot. Each data point represents the median ±1 SD for 10–12 female flies (*UAS-GFP;;OK107-Gal4*) that underwent laser surgery 6 d following eclosion. (*L* and *M*) Two-photon images of *UAS-GFP;;OK107-Gal4* flies after manual dissection (*L*) or after laser surgery (*M*). For both images the laser power (920-nm wavelength) at the specimen plane was 3 mW. (Scale bars, 5 μm.)

whether these lasers can open optical windows in an organism's exoskeleton for in vivo microscopy.

Here we report a largely automated microsurgery protocol that uses a nanosecond-pulsed UV excimer laser to gain optical access to the brain. Our approach enables swift (<1 s) removal of the exoskeleton and precise cuts of high repeatability. These are general capabilities that we illustrate here in three invertebrate species. We also demonstrate surgical incisions in the mouse cranium with sizes and spacings that are infeasible using drills and scalpels.

In flies, we used a phototaxis assay to show that our surgical technique can be performed with minimal to no measurable impact on fly behavior. Microsurgical removal of the cuticle facilitates in vivo imaging of neuronal Ca^{2+} dynamics, as illustrated here in olfactory neurons. Microsurgery is also sufficiently gentle to permit intravital imaging over extended time periods, as demonstrated by our Ca^{2+}-imaging studies of Kenyon cells in the fly mushroom body for up to 18 h.

Results

We chose our laser wavelength and pulse duration to affect fly behavior minimally and avoid photobleaching fluorescent markers just beneath the cuticle. Initial tests with a 355-nm laser showed that this wavelength induced substantial photobleaching. However, UV laser ablation with an excimer laser of 193-nm wavelength seemed suited to our needs (Fig. 1*B*) because photons of this wavelength can break covalent bonds but have an absorption length in water of <1 μm (13). Thus, tissue absorbs the UV energy within a very shallow surface layer, and the superheated material is ejected before thermal energy diffuses to surrounding areas (14). We reasoned that this should avoid photobleaching beneath the ablated layer because fluorophores more than a few microns below the cut surface receive a tiny fraction of the incident light intensity.

Microfabricated, Silicon Mounts Facilitate Rapid Presurgical Preparation. For the first step of the surgical protocol we developed means to quickly fix a fly's body in place while permitting its legs and wings to move freely (Figs. S1 and S2 and Movie S1). To do this, we used UV-cured epoxy to attach the fly to a 125-μm-diameter silica fiber. The fiber lay in a precision-etched V groove created within a silicon wafer (*SI Materials and Methods*). The fixture was designed to be compatible with a set of robotic techniques for fly handling that we are also developing to further speed experimental throughput.

We positioned the fly with ~25-μm repeatability in all three spatial dimensions relative to fiduciary marks etched in the silicon wafer and the well-defined depth of the V groove (Figs. S1 and S2). We placed a metal strip with an 800-μm-diameter opening on top of the fly. This opening provided optical and fluidic access to the fly, allowing us to immerse exposed tissue in saline immediately after surgery (*Materials and Methods*).

A Flexible Microdissection Protocol Based on Laser Percussive Drilling. In mounted flies positioned under a UV-compatible objective lens (Fig. 1*B*), we examined whether nonscanning, laser percussive drilling (15) allowed dissection of the fly cuticle or if a laser-scanning approach was necessary.

Percussive drilling offers superior cutting speed but requires sufficient pulse energy to drill in parallel all subregions within the area demarcated for ablation. We found that the thickness of the fly cuticle is sufficiently uniform that percussive drilling can precisely create a window in the cuticle over the entire ∼0.1-mm^2 area illuminated by the surgical laser (275 mJ/cm^2) (Fig. 1 *C–F*), without ablating underlying brain tissue. With <1 s of drilling, laser pulses of 200 μJ delivered at 100 Hz removed a 300-μm-diameter window in the cuticle. We thus chose this mode of microsurgery rather than laser-scanning approaches, which would have required additional hardware for scanning and much higher laser repetition rates (e.g., ∼3 orders of magnitude higher for a ∼10-μm-diameter laser spot) to achieve the same rate of tissue removal. Our surgery station allowed us to select the size and shape of the ablation by using different apertures or masks that were placed in the laser beam's delivery pathway and projected onto the cuticle surface (Fig. 1 *B–E*). The edges of the laser cuts in tissue were locally straight; electron microscopy studies of postsurgical specimens revealed ≤100 nm of orthogonal deviation from the straight edges (Fig. 1*G*). Tissue structures as near as 2 μm to the surgical cuts appeared unaltered (Figs. 1 *G–I*), and laser microsurgery readily created holes as tiny as ∼12 μm in diameter (Fig. 1 *H* and *I*).

For tailoring surgeries to different parts of the fly brain, we attached flies to the silica fiber in different orientations and adjusted the laser pulse energy and beam size as needed (Fig. 1*B*). With the fiber on the side of the fly's neck, we accessed visual neurons that are challenging to expose manually in live flies (Fig. 1*J* and Movie S2). To access olfactory neurons, we attached the fiber at the nape of the fly's neck. To monitor the depth of surgical ablation, we used a 470-nm-wavelength, fiber-coupled light-emitting diode (LED) to excite green fluorescent protein (GFP) markers. For example, in flies expressing GFP in the mushroom bodies (*UAS-GFP;;OK107-Gal4*), fluorescence signals rose monotonically across the first ∼120 excimer laser pulses (200 μJ), indicative of cuticle removal, but then declined as additional pulses ablated brain tissue (Fig. 1*K*).

Laser Microsurgery Requires Seconds for Dissections with Submicron Precision. We tested the laser surgery system in several ways. As a test of cutting speed and throughput, we mounted four flies (*UAS-GFP;;OK107-Gal4*) on an individual silicon wafer (Fig. S2*B*). Using motorized translation stages to rapidly address each of the four flies, we opened a 300-μm-diameter window in each cuticle and acquired a fluorescence image of the mushroom bodies. Cutting and imaging took 22 s for all four flies in total.

A second test of our surgical system concerned the aspect ratio of the holes it can cut in tissue (Fig. S3). We successfully drilled a constant, 35-μm-diameter hole through the entire ∼400-μm-thick fly, without adjusting the fly's position en route. This aspect ratio is generally unachievable by laser cutting systems that rely on high-numerical aperture (NA) objective lenses, as typically used with near-infrared ultrashort-pulsed laser sources (8, 9).

A third test assessed whether excimer laser surgery induced photobleaching of the GFP markers in the brain. We used two-photon microscopy to inspect five flies (*UAS-GFP;;OK107-Gal4*) expressing GFP in mushroom body olfactory neurons. These cells are among the most commonly examined in flies for studies of olfactory sensing, learning, and memory (7). We manually dissected the cuticles of two of the flies and used laser microsurgery on the other three (120 pulses). Using identical imaging parameters for all five flies, fluorescence signals from all of the flies were comparable to within ∼15%. The difference in mean signal intensity (averaged in each fly over several dozen Kenyon cells of the mushroom bodies) between the two manually dissected samples (∼15%) was comparable to the variation between the mean intensity from the two manually dissected flies and that from the three laser-cut flies (∼13%), suggesting that the variation in GFP expression between flies was greater than any bleaching potentially induced by laser surgery (Fig. 1 *L* and *M*).

Last, we tested the applicability of our methods to other species. We attained comparable precision when cutting windows in the cuticle of the harvester ant (Fig. S4) and *Caenorhabditis elegans* (Fig. S5). Beyond invertebrates, manual dissection can be equally challenging in vertebrates and is often a stumbling block in mammalian neuroscience. Thus, we examined whether excimer laser surgery was effective in the mouse cranium. Strikingly, we found that with ∼3 s of pulsed illumination we could cut precise, square openings (∼100 μm across) through the entire depth of the cranium (Fig. S6).

Optical Parameters for Minimal Impact on Fly Behavior. To gauge the impact of laser surgery on fly behavior, we subjected hundreds of wild-type flies to various numbers of laser pulses, ranging from 0 to 100. We delivered all pulses at the same repetition rate and with identical spot sizes (275-μm diameter) and energies (170 μJ) to a portion of cuticle centered over the antennal lobes. Following microsurgery we used a T-maze to monitor the flies' phototactic responses to a light source that is normally attractive (Fig. 2). This tested for deficits in the sensory integration motor pathway (16). We included in this test some flies in which we additionally used laser surgery to cut muscle 16, which reduces brain motion during in vivo imaging.

Flies that received up to 90 laser pulses maintained statistically significant phototactic responses, whether or not muscle 16 was cut [for <80 pulses, $P < 3 \times 10^{-5}$, $n = 141$ flies; for 80 pulses,

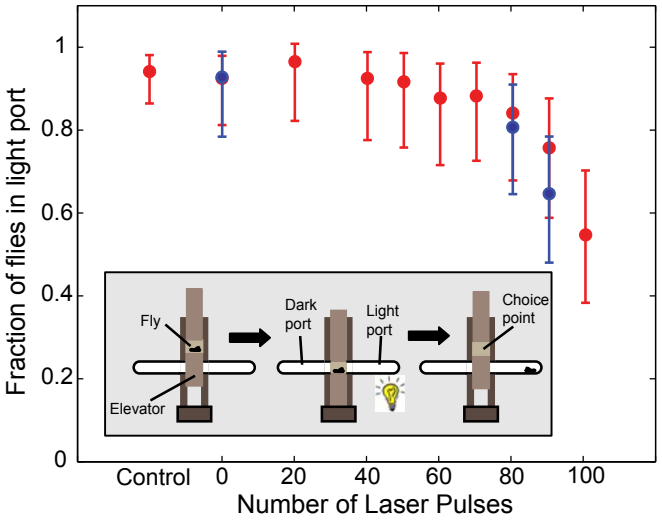

Fig. 2. Fruit flies retain normal phototactic behavior following surgery with a near-optimal number of laser pulses for maximizing postoperative fluorescence signals. After laser microsurgery with ≤80 laser pulses, flies showed no significant performance differences compared with either control flies that underwent only phototactic testing or flies that were mounted but received zero laser pulses. Red and blue data points indicate flies that had muscle 16 uncut and cut, respectively (*Materials and Methods*). Error bars indicate 90% confidence intervals using the adjusted Wald method for two-tailed binomial distributions. (*Inset*) The T-maze phototaxis assay involves loading the fly into an elevator apparatus, lowering the elevator to the choice point and illuminating one of two ports in the T-apparatus, raising the elevator after a set amount of time, and determining where the fly is located.

$P = 1.2 \times 10^{-4}$, $n = 24$ flies (muscle uncut), and $P = 1.5 \times 10^{-4}$, $n = 25$ flies (muscle cut); for 90 pulses, $P = 1.8 \times 10^{-3}$, $n = 24$ flies (muscle uncut), and $P = 8.2 \times 10^{-3}$, $n = 25$ flies (muscle cut); and for 100 pulses, $P = 0.067$, $n = 24$ flies (muscle uncut); two-tailed adjusted Wald binomial test]. Further, flies that underwent the mounting aspects of our protocol and received 0–80 laser pulses had phototactic responses with no significant differences from those of control flies that only received phototactic testing (Fig. 2) [$P = 0.76$ at 0 pulses, $n = 60$ (unmounted flies) and $n = 36$ (mounted flies); $P = 0.16$ at 80 pulses, $n = 36$ (mounted, no surgery) and $n = 24$ (mounted, laser surgery, muscle uncut); and $P = 0.07$ at 80 pulses, $n = 36$ (mounted, no surgery) and $n = 25$ (mounted, laser surgery, muscle cut); Kruskal–Wallis ANOVA]. At a dosage of 90 pulses, flies' phototactic responses showed the first significant differences from control flies [$P = 0.02$, $n = 36$ (mounted, no surgery) and $n = 24$ (mounted, laser surgery, muscle uncut), and $P = 0.002$, $n = 36$ (mounted, no surgery) and $n = 25$ (mounted, laser surgery, muscle cut)]. With 100 laser pulses, phototactic responses declined further (Fig. 2). Thus, for <80–90 pulses, flies' postoperative phototactic responses were statistically indistinguishable from those of control flies.

Two-Photon Ca^{2+} Imaging of Neural Dynamics over Extended Time Periods. We also used two-photon microscopy to record odor-evoked Ca^{2+} transients in the antennal lobe, to assess if laser microsurgery impacted flies' odor-evoked neural responses. We imaged flies (*GH146-Gal4, UAS-GCaMP3*) expressing the Ca^{2+} indicator GCaMP3 in olfactory projection neurons (17), after using 85 UV laser pulses (spot size of 325 μm × 225 μm) to remove cuticle tissue (Fig. 3*A*). GCaMP3 expression was readily visible before odor delivery, and the antennal lobe tissue appeared as normal and healthy as in our prior two-photon imaging studies of manually dissected flies (18) (Movie S3).

The ~25-μm repeatability of our mounting protocol allowed us to quickly locate an optical plane showing several different glomeruli. We then delivered multiple odors to the flies. Analysis of the resulting two-photon images revealed patterns of odor-evoked neural excitation and inhibition that were consistent with prior studies on manually dissected flies (4, 19, 20) (Fig. 3*B*). Olfactory responses were prominent, with changes in GCaMP3 fluorescence ($\Delta F/F$) generally >60% (Fig. 3*C*).

To demonstrate the extension of imaging duration that is attainable via laser microsurgery, we developed a version of the surgical protocol that was particularly minimally invasive and prohibitive by hand dissection. This involved the creation of a smaller opening in the cuticle (120 μm × 90 μm elliptical opening) plus a surrounding annular region in which we thinned but did not remove the exoskeleton (Fig. 4*A*). In this way, we attained optical access to the Kenyon cells of the fly's mushroom bodies (*UAS-GCaMP3/+;OK107-Gal4/+*) via a hole that minimized the impact on fly health while providing adequate transparency across the broader thinned area. This thinned-cuticle strategy allowed us to observe odor-evoked Ca^{2+} dynamics in these neurons even 18 h after laser microsurgery (Fig. 4 *B* and *C*) and to track the same individual cells across 6- to 18-h intervals (Fig. S7). By comparison, we were unable to reproduce these results using manual dissection.

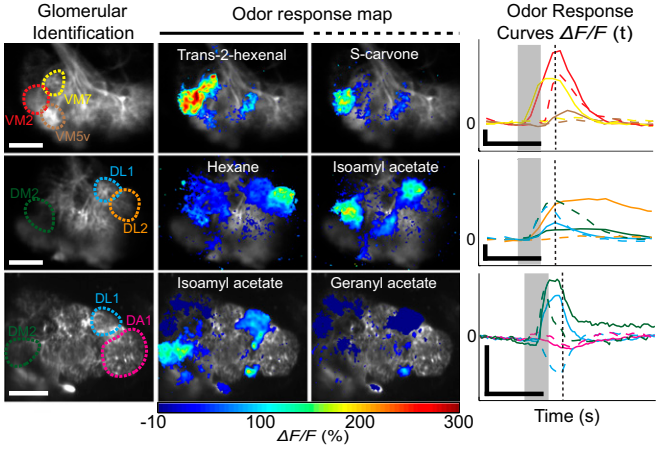

Fig. 3. Two-photon imaging reveals normal odor-evoked neural Ca^{2+} responses in live flies following laser microsurgery. The first column shows baseline two-photon images of three different *GH146-Gal4,UAS-GCaMP3* flies expressing the Ca^{2+} indicator GCaMP3. Several glomeruli are visible, three of which are demarcated with dotted lines. Across flies, glomeruli are labeled consistently by color: VM2, red; VM7, yellow; VM5v, brown; DM2, green; DL1, blue; DL2, orange; and DA1, pink. (Scale bars, 20 μm.) In the second and third columns, maps of odor-evoked fluorescence changes ($\Delta F/F$) reveal glomerular activation following a 2-s pulse of odor delivery, for different pairs of odors. Both excitatory and inhibitory glomerular responses occurred. Odor-evoked fluorescence changes are indicated in color for regions where the response absolute value was at least three times greater than the standard deviation of baseline fluctuations. The fourth column shows traces of odor-evoked changes ($\Delta F/F$) for the three encircled glomeruli and two odors indicated in each row. Colors match those of the glomeruli in the first column. Solid and dashed lines are for the odors indicated in the second and third columns, respectively. Odor delivery occurred at times marked by gray bars. Dashed black line indicates the time point shown in the second and third columns. Vertical and horizontal scale bars are 100% $\Delta F/F$ and 5 s, respectively.

Discussion

We developed an excimer laser microsurgery protocol that can rapidly and precisely remove fly cuticle with minimal impact on fly behavior or underlying fluorescent markers. Our approach obviates the highly variable outcomes of manual dissection by providing repeatable, user-friendly, and rapid laser-cutting capabilities with ~100-nm-level precision.

Traditional scanned UV laser ablation setups that operate at a wavelength of 355 nm (21) suffer from longer absorption depths, causing fluorophore bleaching in the brain. In comparison with surgical systems based on ultrafast laser sources, the cost of our instrumentation was ~2–5% the price of a commercial two-photon microscope equipped with a Ti:sapphire laser amplifier. These amplifiers typically require considerable effort to maintain intracavity alignment, but excimer lasers are widely used in medicine and exist in user-friendly versions.

Our surgical success with flies, ants, and nematodes indicates that research involving a range of small model organisms should benefit from our methods. Moreover, our capability to cut through the mouse cranium in ~3 s suggests that excimer laser surgery has substantial utility for research on mammals. Excimer lasers with higher energies are commercially available, so cranial openings larger than those illustrated here could also be created percussively. The cranial openings we cut had sharp corners that would be nearly impossible to create manually, certainly not within seconds.

Indeed, a striking advantage of our laser microsurgery system over manual dissection is our ability to cut holes of arbitrary shape, size, and depth. Our low-NA system can readily create high-aspect ratio holes of small diameter. In flies, mice, or other species, this capability may ease minimally invasive injections or electrical recordings. In imaging experiments, the traditional manual approach of removing the cuticle generally requires making an opening larger than the imaging field of view, to avoid damaging the brain area of study. The larger window in the cuticle constitutes a greater insult to the fly, and the resulting declines in the fly's health reduce the total time available for imaging neural responses, typically 1 to several hours (1, 2, 7, 18).

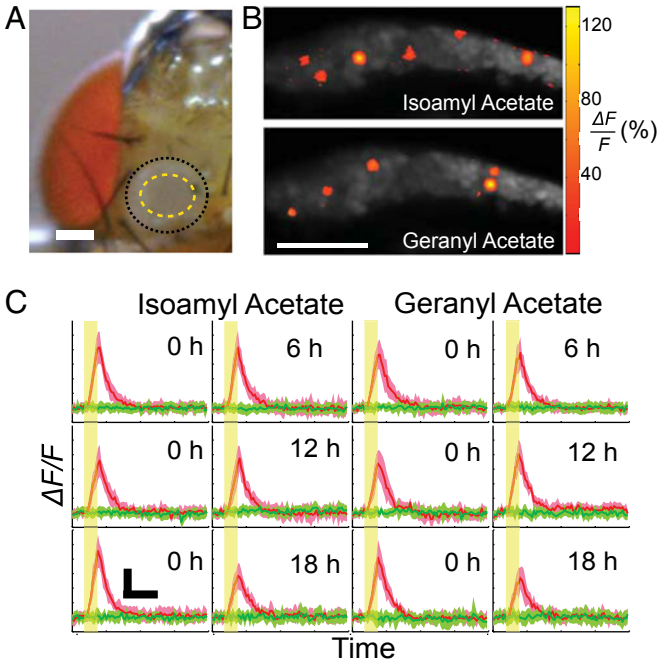

Fig. 4. Minimally invasive microsurgery allows observation of robust, odor-evoked Ca^{2+} signals in Kenyon cells for up to 18 h. (*A*) Bright-field image of a *UAS-GCaMP3/+;OK107-Gal4/+* fly following laser microsurgery. The yellow dotted line outlines the portion of the cuticle that was removed. To improve fluorescence collection, the cuticle of the surrounding annulus (out to the black dotted line) was also thinned. (Scale bar, 100 μm.) (*B*) Odor-evoked activation of individual Kenyon cells 6 h after surgery. (Scale bar, 25 μm.) (*C*) Odor-evoked fluorescence changes in Kenyon cells for flies imaged at different time points. For each fly, the three cells with the largest Δ*F*/*F* signals for a given odorant were measured at each time point. These responses were averaged across all flies studied and plotted in red ($n = 6$ flies at 6 h, $n = 4$ flies at 12 h, and $n = 4$ flies at 18 h). For comparison, mean responses of these same cells to a control odor (mineral oil) at the same time points are shown in green. Shaded areas surrounding the mean response curves indicate SDs. Odor delivery occurred at times marked by yellow bars (2-s duration). Horizontal and vertical scale bars are 5 s and 40% Δ*F*/*F*, respectively.

The minimally invasive capabilities of our surgical approach have allowed the longest time-lapse imaging studies of neural activity in live flies reported to date. For these studies we thinned the cuticle over a ∼200-μm-wide region and created a central opening (∼100 μm) smaller than possible by hand. The resulting 6- to 18-h imaging durations so attained represent a ∼4- to 18-fold extension compared with prior studies; this is a notable improvement because the durations attainable via laser microsurgery now suffice to study many unanswered questions in neuroscience, such as those involving neuronal plasticity or the neurobiology of learning and memory.

After mounting a fly, our entire surgical protocol takes only ∼10 s, of which ∼1 s is devoted to laser pulse delivery. With four flies mounted on the same silicon wafer, we completed all four surgeries in 22 s, indicating the amenability of our methods to high-throughput experimentation. By capitalizing on silicon wafers of larger diameter than those used here, our four-fly mount should be extendable to greater numbers of flies, such as for parallelization of neural imaging studies. Our protocol also allows flies to be mounted with high precision, which reduces the alignment time at subsequent surgery and imaging steps.

Given this speed and efficiency of throughput, our methodology should be able to facilitate future high-throughput screens for flies with mutant cellular, functional, or anatomical phenotypes. We are developing robotic techniques that use automated machine vision algorithms to further reduce the time it takes to pick and mount flies for surgery and imaging. Further, by integrating interferometric measurements of the cutting depth into the surgical process, it might be possible to remove the fly's perineural sheath without damaging underlying brain structure, such as for electrophysiological studies. Similarly, it should be possible to create a preparation in which the fly cuticle is left entirely unopened and merely thinned for imaging, to further extend the duration of time-lapse experiments. We chiefly focused here on fruit flies, but our precise and repeatable capabilities to create optical windows in nearly any part of an animal's body should be widely applicable in multiple biological disciplines and to invertebrates and vertebrates alike.

Materials and Methods

Fly Stocks. We crossed *GH146-Gal4* and *UAS-GCaMP3* fly lines (2) to label olfactory projection neurons in the antennal lobe. We crossed *OK107-Gal4* with *UAS-GFP* and *UAS-GCaMP3* lines to label mushroom body neurons. We raised all flies on standard cornmeal agar media under a 12-h light/dark cycle at 25 °C and 50% humidity. All experiments used adult mated females.

Fabrication and Use of Silicon Mounting Fixtures. We made silicon (Si) fixtures in Stanford's Ginzton microfabrication facility. We used <100>-crystallographic orientation, 4-inch-diameter, 500-μm-thick, single-side polished Si wafers with 100 nm of low-stress nitride on both sides (University Wafer). *SI Materials and Methods* contains detailed microfabrication methods and description of how we mounted the fly to the silica fiber and the fiber to the Si wafer. It took ∼60 s to fix the fly's position with ∼25-μm accuracy relative to the etched holes in the silicon. The fly was free to move its legs and wings when attached to the fiber (Movie S1).

Laser Surgery System. We used Optex and GamLaser EX5 ArF 193-nm excimer lasers, each capable of generating ∼12-mJ pulses of ∼10-ns duration. The total exposure time of the cuticle to the laser was <1 s, so the fly's haemolymph would not have time to flow into the machined hole and shield the fly's air sacs from the laser pulses. A 250-mL/min flow of air from a 6-mm-diameter tube aimed just above the fly prevented deposition of ejected debris on the objective lens. To control the beam shape and spot size on the fly, we used various pupil masks consisting of gold-coated thin copper substrates that were laser machined to have the desired aperture (National Aperture). We projected the aperture with 3× demagnification onto the fly using a CaF_2 lens with a 40-mm focal length at 193 nm.

Fly Surgical Protocol. After transferring a mounted fly to the surgery station, we measured fluorescence signals using a photoreceiver (Newport 2151) and a 515/20 band pass optical filter (Semrock). For imaging certain brain regions, we reduced brain movement by laser drilling a 50-μm-diameter hole (6 μJ, 1,400 pulses, 200 Hz) between the fly antennae to cut muscle 16. We then opened the optical window in the cuticle. Immediately after surgery, we applied 90 μL of adult haemolymph-like (AHL) saline (103 mM NaCl, 3 mM KCl, 5 mM TES, 1 mM NaH_2PO_4, 1.5 mM $CaCl_2{\cdot}6H_2O$, 4 mM $MgCl_2{\cdot}6H_2O$, 26 mM $NaHCO_3$, 10 mM sucrose, 10 mM trehalose, and 10 mM glucose; all from Sigma in the highest purity). This prevented the brain from desiccating, and the surface tension of the AHL on the hydrophobic fly cuticle prevented AHL from spilling on the fly's body. The entire surgery took ∼10 s.

Behavioral Testing. *SI Materials and Methods* provides details of the phototaxis studies.

Two-Photon Microscopy. To image the antennal lobe, we used a custom-built two-photon microscope and a 20× water-immersion objective (0.95 NA; Olympus). The excitation powers (920-nm wavelength) at the specimen were 3 mW and 15 mW for Figs. 1 *L* and *M* and 3, respectively. The pixel dwell time was 2 μs. For imaging mushroom bodies, we used a 40× water-immersion objective (1.0 NA; Zeiss) and a commercial two-photon microscope (Prairie Technologies). The excitation power (927 nm) at the specimen was 10–18 mW for Fig. 4. The pixel dwell time was 1.2 μs for all images.

Time-lapse imaging. Our protocol requires that to maximize reproducibility for a given laser microsurgery recipe (pulse energy, number of pulses, repetition rate, and size of the window), the cuticle thickness and composition should vary as little as possible from fly to fly. Thus, we used flies of identical age (2-d-old mated females) and reared them under uniform growth conditions, with the same number of parent flies in each vial (10 female Oregon-R and 3 male

UAS-GCamP3/CyO;OK107-Gal4) and fresh food. We collected flies twice a day to maintain <10 female and <5 male offspring per vial.

During laser surgery (60 laser pulses; ~275 mJ/cm^2 per pulse), we translated the fly out of focus to blur the edges of the cut; this approach fully removed the cuticle at the center of the cut but merely thinned it in the periphery. We did this to minimize the exposed brain area, maximize the collected fluorescence, and remove a sufficient area of cuticle for adequate tissue contact with the subsequently applied AHL. Following surgery, we perfused flies with oxygenated AHL in a humidified enclosure.

All flies underwent two-photon imaging immediately after surgery. Flies with clearly resolved brain structures (~60% of all flies in the first session) were imaged at one additional later time point (6 ± 1 h, 12 ± 1 h, or 18 ± 1 h) and were included in the analyses of the time-lapse experiments. The poor resolution of brain structures in the other ~40% of flies that we discarded was caused by either excessive brain movement (~20% of flies in the initial session), partial obscuring of the mushroom body structures due to lateral and/or angular misalignments (~15% of all flies in the initial session), or incomplete cuticle removal (~5% of flies). During imaging, flies received a single, 2-s pulse of odor within a 40-s interval. To minimize bleaching, we imaged for 20 s of each of the four 40-s trials for each odorant. We averaged the data from the four trials for subsequent analyses. Of the flies designated for reimaging at 18 h, ~20% survived the 18-h wait from the first imaging session.

Analysis of Ca^{2+}-imaging data. We converted the raw 16-bit images to 32 bits using ImageJ [National Institutes of Health (NIH)] and registered images in the two lateral dimensions using an ImageJ plugin (22). For both antennal lobe and mushroom body images, we averaged all movie frames before odor stimulus delivery to assess baseline fluorescence. For all raw images, we applied a spatial, low-pass Gaussian filter with a radius of either 2 pixels (for 256×256 pixel images) or 4 pixels (512×512 images). We additionally applied a temporal smoothing filter (sliding window of one frame) to the mushroom body images.

To analyze the time-lapse Ca^{2+}-imaging data in the mushroom bodies, for each session we computed the $\Delta F/F$ traces. We median filtered (3×3 array) the $\Delta F/F$ data and applied a uniform threshold to discard pixels at or below background fluorescence levels. In Fig. 4, pixels with >30% $\Delta F/F$ odor responses are superimposed on the basal fluorescence images. We manually selected the three cells with the largest odor-evoked fluorescence signals ($\Delta F/F$) for each image sequence. We used a 6×6 pixel window and a custom MATLAB script to average the signals in this window at each frame across an odor delivery trial. This window size helped average out pixel noise within a frame but remained within the area of one cell (~20×20 pixels). All calcium-imaging experiments used four odor puff cycles, and we considered responses as valid only if they were present in at least two cycles. For z stacks, we averaged eight frames per slice. We performed all statistical tests in MATLAB (MathWorks).

Mice. The Stanford Administrative Panel on Laboratory Animal Care approved all procedures. See *SI Materials and Methods* for surgical details.

ACKNOWLEDGMENTS. We thank D. Clark, J. Savall, L. Burztyn, M. Horowitz, M. Scott, T. Clandinin, K. Shen, T. Carver, and G. Dietzl for helpful conversations; and J. Li, J. Simon, G. Dietzl, S. Sturgis, and X. Wei for technical assistance. We also thank L. Looger, K. Shen, and D. Gordon for kindly providing the UAS-GCaMP3 flies, nematodes, and ants, respectively. The W. M. Keck Foundation, the Stanford Bio-X program, and an NIH Director's Pioneer Award supported our research.

1. Tuthill JC, Chiappe ME, Reiser MB (2011) Neural correlates of illusory motion perception in Drosophila. *Proc Natl Acad Sci USA* 108(23):9685–9690.
2. Seelig JD, et al. (2010) Two-photon calcium imaging from head-fixed Drosophila during optomotor walking behavior. *Nat Methods* 7(7):535–540.
3. Ng M, et al. (2002) Transmission of olfactory information between three populations of neurons in the antennal lobe of the fly. *Neuron* 36(3):463–474.
4. Wang JW, Wong AM, Flores J, Vosshall LB, Axel R (2003) Two-photon calcium imaging reveals an odor-evoked map of activity in the fly brain. *Cell* 112(2):271–282.
5. Gouwens NW, Wilson RI (2009) Signal propagation in Drosophila central neurons. *J Neurosci* 29(19):6239–6249.
6. Yorozu S, et al. (2009) Distinct sensory representations of wind and near-field sound in the Drosophila brain. *Nature* 458(7235):201–205.
7. Wang Y, et al. (2004) Stereotyped odor-evoked activity in the mushroom body of Drosophila revealed by green fluorescent protein-based Ca2+ imaging. *J Neurosci* 24(29):6507–6514.
8. Nguyen J, et al. (2011) Sub-surface, micrometer-scale incisions produced in rodent cortex using tightly-focused femtosecond laser pulses. *Lasers Surg Med* 43(5):382–391.
9. Tsai PS, et al. (2003) All-optical histology using ultrashort laser pulses. *Neuron* 39(1):27–41.
10. Yanik MF, et al. (2004) Neurosurgery: Functional regeneration after laser axotomy. *Nature* 432(7019):822.
11. Fuhr G, et al. (1999) UV-laser ablation of sensory cells in living insects. *Appl Phys A Mater Sci Process* 68(4):379–385.
12. Pallikaris IG, Siganos DS (1994) Excimer laser in situ keratomileusis and photorefractive keratectomy for correction of high myopia. *J Refract Corneal Surg* 10(5):498–510.
13. Pettit GH, Ediger MN (1996) Corneal-tissue absorption coefficients for 193- and 213-nm ultraviolet radiation. *Appl Opt* 35(19):3386–3391.
14. Venugopalan V, Nishioka NS, Mikić BB (1995) The thermodynamic response of soft biological tissues to pulsed ultraviolet laser irradiation. *Biophys J* 69(4):1259–1271.
15. Dubey AK, Yadava V (2008) Laser beam machining—A review. *Int J Mach Tools Manuf* 48(6):609–628.
16. Zhu Y, Nern A, Zipursky SL, Frye MA (2009) Peripheral visual circuits functionally segregate motion and phototaxis behaviors in the fly. *Curr Biol* 19(7):613–619.
17. Tian L, et al. (2009) Imaging neural activity in worms, flies and mice with improved GCaMP calcium indicators. *Nat Methods* 6(12):875–881.
18. Liang L, et al. (2013) GABAergic projection neurons route selective olfactory inputs to specific higher-order neurons. *Neuron* 79(5):917–931.
19. Hallem EA, Carlson JR (2006) Coding of odors by a receptor repertoire. *Cell* 125(1):143–160.
20. Bhandawat V, Olsen SR, Gouwens NW, Schlief ML, Wilson RI (2007) Sensory processing in the Drosophila antennal lobe increases reliability and separability of ensemble odor representations. *Nat Neurosci* 10(11):1474–1482.
21. Espina V, Heiby M, Pierobon M, Liotta LA (2007) Laser capture microdissection technology. *Expert Rev Mol Diagn* 7(5):647–657.
22. Nimmerjahn A, Mukamel EA, Schnitzer MJ (2009) Motor behavior activates Bergmann glial networks. *Neuron* 62(3):400–412.

Supporting Information

Sinha et al. 10.1073/pnas.1216287110

SI Materials and Methods

Silicon Fixtures. We used a laser-printed mylar mask with 3-μm resolution (Artnet Pro) to define the features of the fly holder on the Si wafer. In addition to the V groove for the fiber and the hole for the fly, the mask had four additional holes serving as positional fiducials during fly mounting. After we had spun and patterned the photoresist with the mask, we etched the exposed nitride in a plasma etcher. We then used acetone (Sigma) to remove the residual photoresist, placed the wafer into a beaker, submerged it in a 25% wt potassium hydroxide solution (with ~5% vol isopropanol) heated to 90 °C and with continual stirring until the wafer had been etched through. We cleaned the wafer and diced it using a wafer saw. One 4-inch-diameter wafer yielded 13 Si mounts, each of which could be reused.

Of the four fiducial holes in each fixture, we used the two rear holes as tight-fit holes to index the Si mount to an underlying brass mount (Fig. S1*C*). We also used this brass mount, which is mechanically sturdier than the Si mount, as a carrier for the Si fixture so that we could move the fly from the mounting stage to the laser microsurgery stage and then later to the two-photon microscope. We used the two front fiducial holes in the silicon fixture to index the brass piece and as the fixture for a metal holder that we placed between the fly's head and the objective lens of the two-photon microscope. We machined this metal holder from 127-μm-thick stainless steel shim stock and included an 800-μm-diameter center hole that provided optical access to the fly brain. We used two 380-μm-thick stainless steel washers, one glued to the underside of each end of this metal holder, as spacers between the top of the silicon fixture and the underside of the stainless steel shim.

Mounting Flies on Fixtures. We transferred flies from stock supplies to a plastic vial held in a container of crushed ice. Once the flies were immobile, we tapped the flies out from the vial onto a shallow petri dish also resting on crushed ice. We turned on the thermoelectric cooler on the mounting apparatus (Fig. S2) to cool the underlying aluminum (Al) block to ~4 °C.

Before mounting each fly, we wiped the Al block to remove condensation. We transferred the fly from the petri dish to the cooled Al surface using a dull pair of forceps to grab onto the base of the wing. The Al block was seated on a translation and rotation multiaxis stage that had six degrees of freedom to allow the user to position the fly relative to the silicon fixture. We placed the fly such that its dorsal side contacted the Al block, with its body centered to the small hole (~350-μm diameter) on the surface of the Al block (Fig. S2). We turned on a weak vacuum (~15 inches of Hg) to prevent the fly from rolling over during subsequent handling steps. We secured the Si mount above the fly, with the 125-μm fused silica fiber taped into the groove using Kapton tape or with removable UV-cured epoxy (Norland Block Adhesive 107).

Using the multiaxis stage, we adjusted the position and angle of the fly in the three translational axes and in the roll and yaw rotational axes, respectively, underneath a dissecting microscope at 40× magnification. We brought the fiber into contact underneath the fly proboscis so that all of the fly's legs were on the same side of the fiber. We applied a small drop of Norland 89 UV epoxy to the fly to secure the fiber to the head and to the proboscis. Securing the proboscis to the rigid structure of the fiber eliminated most discernible brain movement. We cured the epoxy with UV light for 10 s. After curing, we switched off the vacuum and lowered the multiaxis stage.

If we needed to access the fly brain from a different angle, we could then rotate the fly in the pitch axis by removing the tape, turning the fiber within the groove, and replacing the tape when the fly reached the desired angle. We could also rotate the fly about its body axis before it was attached to the fiber. After attachment, the fly was free to move its legs and wings (Movie S2). We then placed the silicon fixture onto the brass mount. Finally, we placed the stainless steel shim holder, which had an opening for optical access to the fly brain, on top of the fly through the front dowels of the brass mount. We usually needed ~60 s total to fix the fly's position with ~25-μm accuracy relative to the etched holes in the silicon. We transferred the fly to the surgical station by placing the brass mount with the indexed silicon piece with the fly onto the brass plate, which obviated any manual adjustments to the fly's position at the surgical stage.

Behavioral Testing. We used 6-d-old mated female Oregon-R flies for the behavioral tests. We collected all eclosed male and female flies every morning from our bottles and placed them in new vials (no more than 40 flies per vial) with fresh food. We flipped the flies onto fresh food every day and kept them at 25 °C and 50% relative humidity in an incubator with a 12-h light and 12-h dark cycle. We assumed that 2 d after eclosion, all female flies had been mated. We sorted the flies on a CO_2 pad, discarding the male flies and placing the female flies in vials (35 flies per vial). We flipped the female flies daily and subjected them to behavioral tests 3 d after sorting.

For behavioral tests, we mounted the flies on steel washers that had fused silica fiber taped to them instead of to the silicon mount. We mounted the flies as before but we did not use the stainless steel metal pieces, and we did not index the washers to the brass piece. After the laser microsurgery, we immediately placed the flies in a polystyrene petri dish with a tight lid (BD-Falcon) that was under a humidification chamber to minimize brain desiccation. We pushed a cotton ball to the bottom of the tube and dropped 1.5 mL of water into the tube. Under a dissecting microscope, we placed the washer on a steel frame that we put on top of the tube. We blew warm humidified air over the washer to prevent evaporation and brain desiccation. We used a razor blade to cut the fiber as close to the fly as possible, and the fly was dropped into the tube. We then quickly removed the steel frame and washer and placed a rubber stopper on top of the tube to form an airtight seal. Flies were able to move quite freely with a short piece of fiber attached to them.

We tested the flies on the T-maze one at a time to prevent the ends of the fiber protruding from one fly from scratching any neighboring flies. We took the tube to a darkened cubicle for the phototaxis test. We maintained the cubicle's temperature and humidity to be 25 °C and 65% relative humidity, respectively. Using a dim red lamp to provide us with sufficient illumination to see, we removed the rubber stopper on the tube and inserted the tube onto the loading port of the T-maze. We encouraged the fly to enter the T-maze elevator, either by the fly's geotaxis response or by gently knocking it. We quickly lowered the elevator to a position between the loading point and the choice point, and we waited 1 min to allow the fly to acclimatize itself to its surroundings.

After 1 min, we switched on a white light-emitting diode on one side of the T-maze and lowered the elevator to the choice point. The white light was scattered through a fine mesh to provide a dim, diffuse source. The fly had 1 min to freely walk between the ports, after which we raised the elevator sufficiently to trap the fly

in the light port, the dark port, or the choice point. We interchanged the tubes used for the light and dark vials every six trials, and we alternated the side of the T-maze that was illuminated by the light source every 12 trials. The total numbers of flies that we assayed for the control condition (i.e., anesthetized but not mounted) and for the simply mounted condition (i.e., anesthetized and mounted but not subjected to UV laser pulses) were 60 and 36, respectively. The number of flies that we assayed for all of the other data points varied between 20 and 25. When using the two-tailed adjusted Wald test for binomial distributions to determine if the flies had a statistically significant phototactic response, we used the null hypothesis that flies would uniformly distribute themselves in the total volume of the dark port, light port, and choice point (the dark port and choice point were combined into one outcome for the statistical test).

Odor Delivery. We delivered odors to the flies via a 3.18-mm-inner-diameter stainless steel tube placed ∼3 mm from the fly antennae. We maintained a constant flow of odorant to the fly and alternatively sourced the airflow from an active odor bottle and a control odor (paraffin oil) bottle using pairs of solenoid valves. We diluted the active odorant in paraffin oil to be 0.1% by volume and delivered the odorant in ∼2 s pulses with a duty cycle ranging from 5% to 10% at a flow rate of 100 mL/min. We constructed all odorant tubes either from Teflon or stainless steel; solenoid valves were Teflon. We kept the tube lengths as short as possible to minimize the total surface area to which odors could stick. We tested different odors sequentially by swapping out the active odorant bottles and tubing and letting the system run for about 40 s to flush out the previous odor before acquiring images for the next odor.

Scanning Electron Microscopy. Following laser microsurgery, we immediately soaked the flies in ethanol for ∼1 d and then dried the flies. We coated the samples with 50–100 Å of gold/palladium alloy and acquired images using a Hitachi S-3400N scanning electron microscope with a 10-kV beam.

Mouse Surgery. Before surgery, we anesthetized mice (12- to 16-wk-old males) using a ketamine/xylazine mixture (90 mg/kg and 15 mg/kg, respectively, delivered by i.p. injection). Body temperature was maintained using a heating blanket. We exposed the skull and cleaned it with saline solution (0.9% NaCl; Baxter). After stabilizing the mouse using ear bars, we positioned the cranium under the objective lens of the laser surgery system. We then opened a grid of cranial openings (centered at 1.13 mm posterior to bregma, 1.85 mm lateral) using 600 laser pulses (300 μJ energy per pulse, delivered at 200 Hz) to create each hole (3 s per hole).

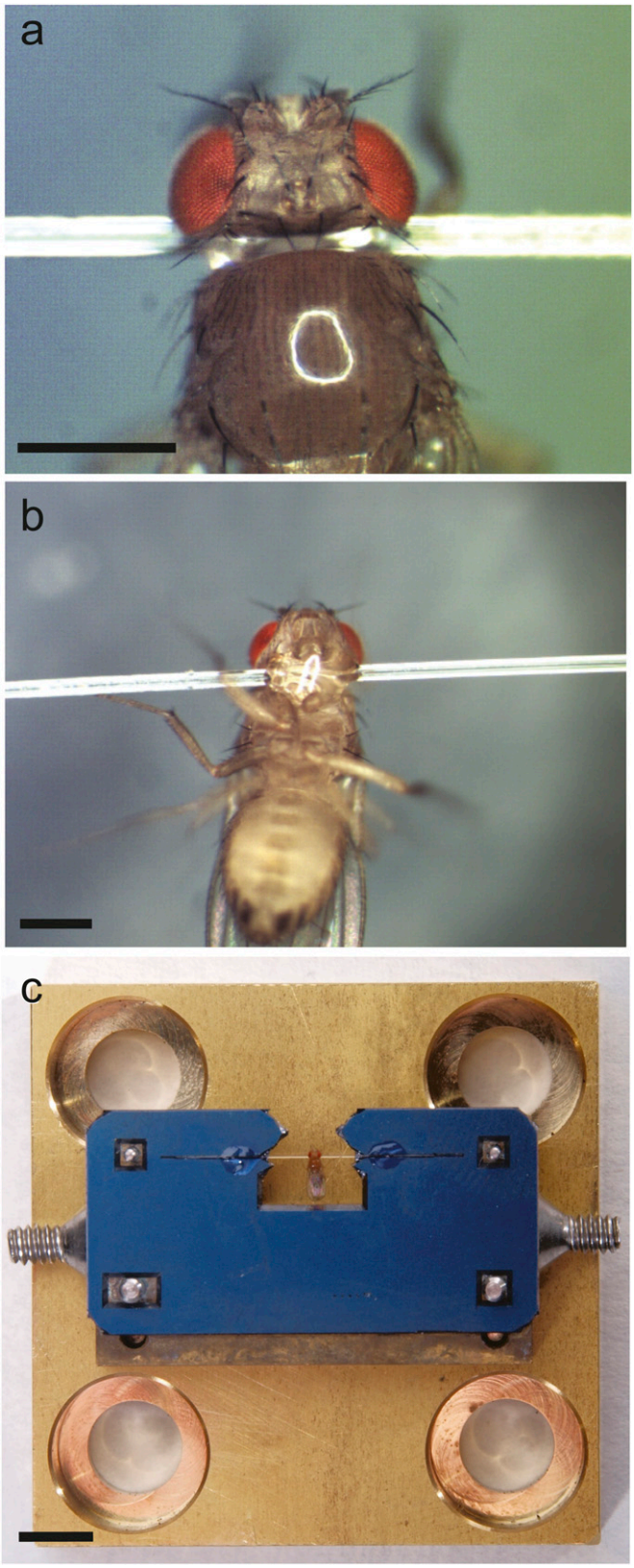

Fig. S1. Photographs of mounted flies. (*A*) Dorsal view of a fly attached to an optical fiber, which in turn is attached to a silicon fixture. A prominent reflection from the illumination is visible on the thorax as a bright loop. (Scale bar, 500 μm.) (*B*) Ventral view of attached fly. (Scale bar, 500 μm.) (*C*) Silicon fixture with fly mounted on brass mount. (Scale bar, 5 mm.)

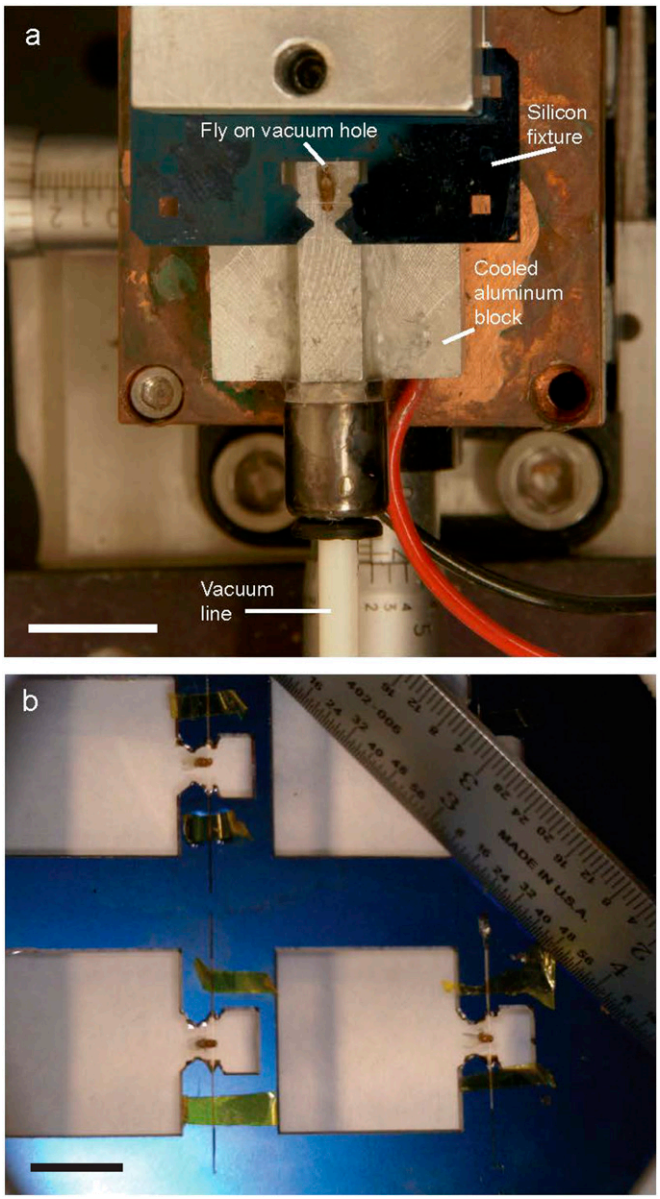

Fig. S2. Fly mounting rig and a mount for multiple flies. (*A*) We placed the fly on a cooled aluminum block and attached it to the fiber (*SI Materials and Methods*). The block sits on a thermoelectric cooler, which in turns sits on a copper heat sink. We affixed the latter to a translation stage with six degrees of motion. (*B*) Silicon holder that has four fruit fly mounts precisely etched with 30-mm spacing in both lateral dimensions. Large rectangular holes were etched around the flies to facilitate stimulus delivery. Without these holes, flies could be packed at greater density. (Scale bars, 10 mm.)

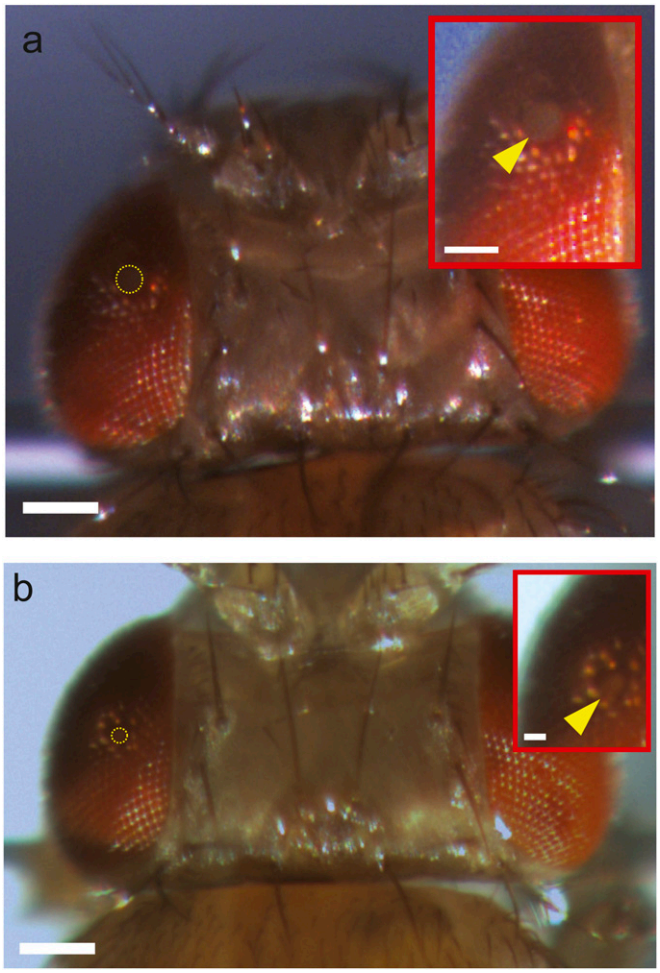

Fig. S3. High-aspect ratio holes cut into *Drosophila melanogaster*. (*A*) A 35-μm-diameter hole (outlined in yellow in the main panel and indicated with a yellow triangle in the inset) cut in the fly eye using 3,000 laser pulses of 4 μJ energy and delivered at 200 Hz. The hole extends through the entire fly eye. (Scale bars, 100 μm and 50 μm in the main panel and inset, respectively.) (*B*) A 20-μm-diameter hole (outlined in yellow in the main panel and indicated with a yellow triangle in the inset) cut in the fly eye using 3,000 laser pulses of 1 μJ energy and delivered at 200 Hz. The hole is ~250 μm deep and was created without scanning the fly's position. (Scale bars, 100 μm and 20 μm in the main panel and inset, respectively.)

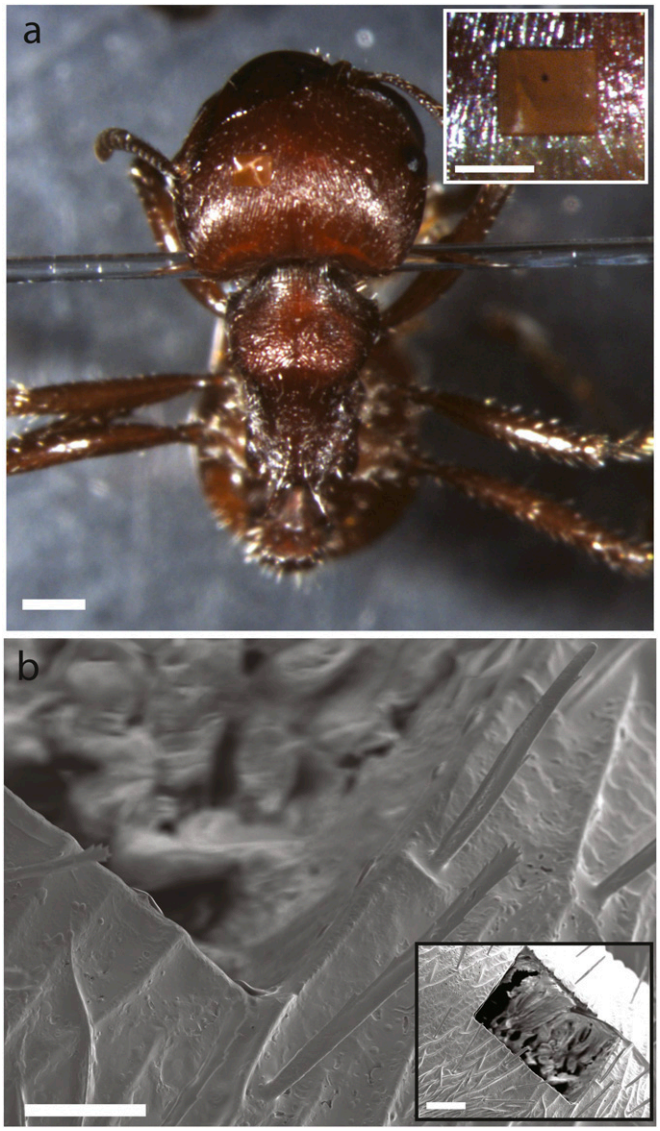

Fig. S4. High-precision laser microsurgery in ants. (*A*) Bright-field image of red harvester ant (*Pogonomyrmex barbatus*) after laser microsurgery. We mounted the ant on a 250-μm-diameter fiber (instead of the 125-μm-diameter fibers used for fruit flies). Inset shows the precisely cut edges of the window in the cuticle created using 300 laser pulses (350 μJ each) delivered at 100 Hz. (Scale bars, 500 μm for the main panel and 250 μm for the inset.) (*B*) Scanning electron micrograph of an ant after laser microsurgery illustrates the clean edges of the cut. Inset shows the rectangular shape of the hole. (Scale bars, 50 μm for the main panel and 100 μm for the inset.)

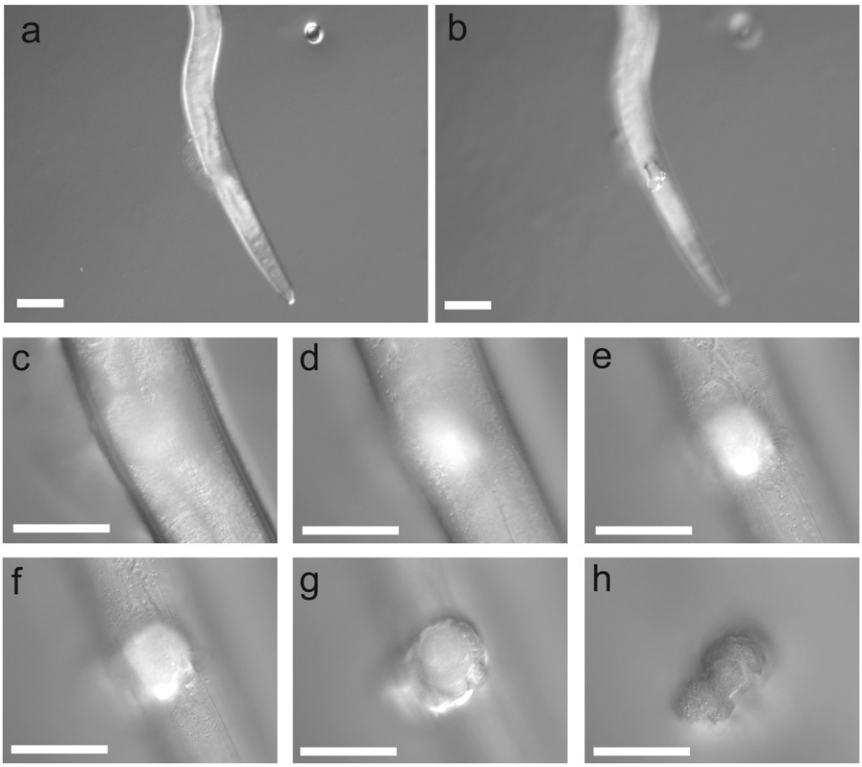

Fig. S5. High-precision laser microsurgery in the *Caenorhabditis elegans*. (*A* and *B*) We cut a 12-μm-diameter hole in *C. elegans* using 15 laser pulses delivered at 100 Hz and each of 0.2 μJ energy. We anesthetized the worm using levamisole on an agarose pad. Images show both the plane of incision (*A*) and a plane above the incision (*B*). (Scale bar, 100 μm.) (*C*–*H*) Differential interference contrast microscopy images of *C. elegans* after surgery. Images are focused at *z* planes that are increasingly distant from the body of the worm from *C* to *H*. (Scale bar, 50 μm.)

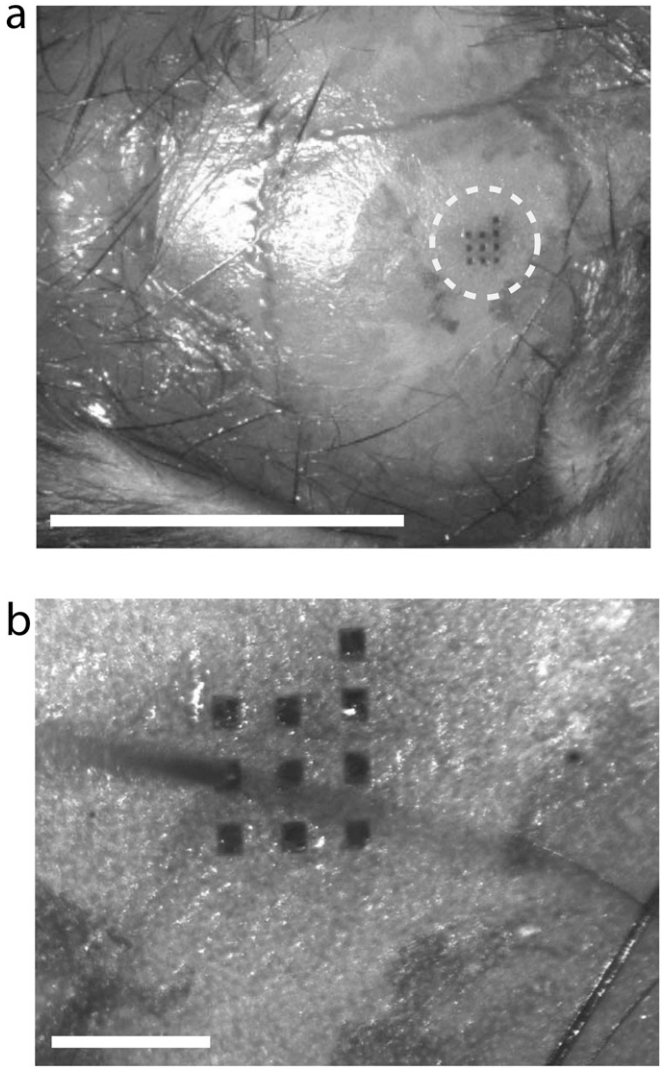

Fig. S6. Grid of holes cut into mouse cranium by laser microsurgery. We laser machined a grid of 10 holes [(3 × 3) + 1] in the cranium of an anesthetized mouse. Each rectangular hole was 95 μm × 110 μm, and the hole spacing was 200 μm in both dimensions. Each hole was created in ~3 s (600 laser pulses at 200 Hz with 300 μJ energy). (*A*) Dotted circle highlights the area of the cranium that underwent surgery. (Scale bar, 5 mm.) (*B*) A tungsten electrode that was 100 μm at its base could be inserted several millimeters into the hole, illustrating complete removal of the bone. (Scale bar, 500 μm.)

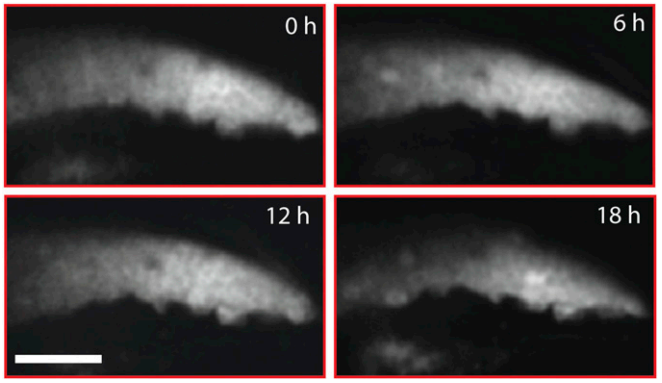

Fig. S7. Time-lapse imaging of mushroom bodies in *UAS-GCaMP3/+;OK107-Gal4/+* flies. After using laser microdissection to thin the cuticle and cut a small central opening (Fig. 4*A*), it was possible to image the same plane of the mushroom body at multiple time intervals in the same fly. We imaged the fly at 6-h intervals. (Scale bar, 25 μm.)

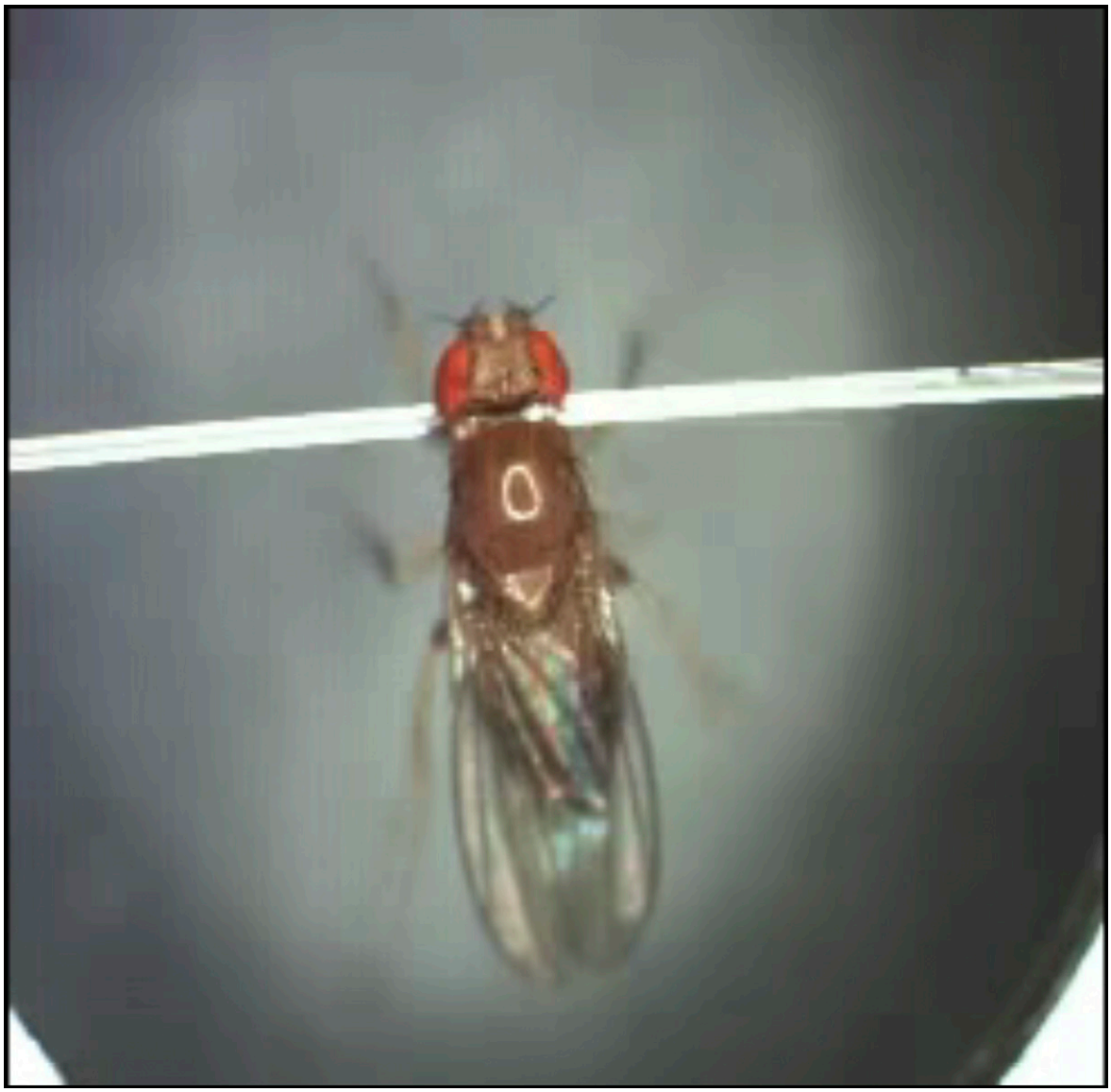

Movie S1. A behaving fly after attachment to the silica fiber. The fly's legs and wings are free to move, but the head remains still.

Movie S1

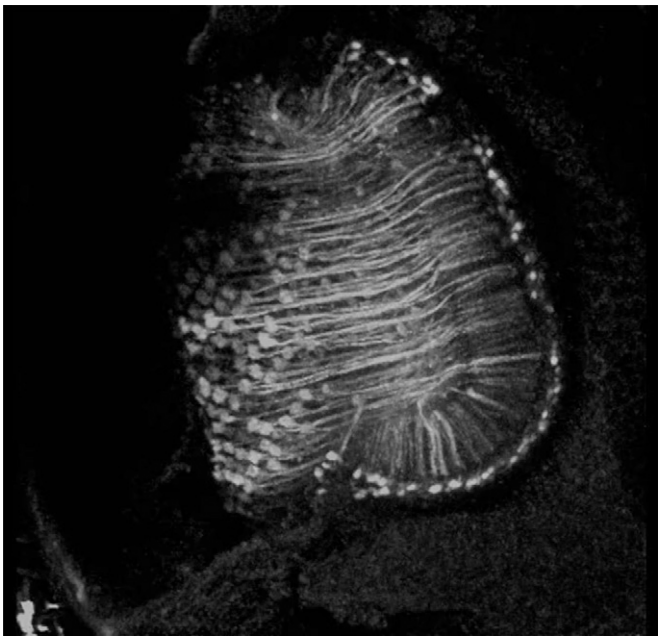

Movie S2. Maximum intensity projections from a 3D stack of images of lamina in a *+/CyO;21DhhGal4,UAS-TNXXLH.3*Z3/TM6B* fly. Each of the 143 slices in the image stack is an average of ten 512 × 512 pixel frames acquired with a 2.4-μs pixel dwell time. The field of view is 275 μm in both dimensions. The axial increment between slices was 1 μm. Laser illumination was 927 nm in wavelength and 15 mW of power at the specimen plane.

Movie S2

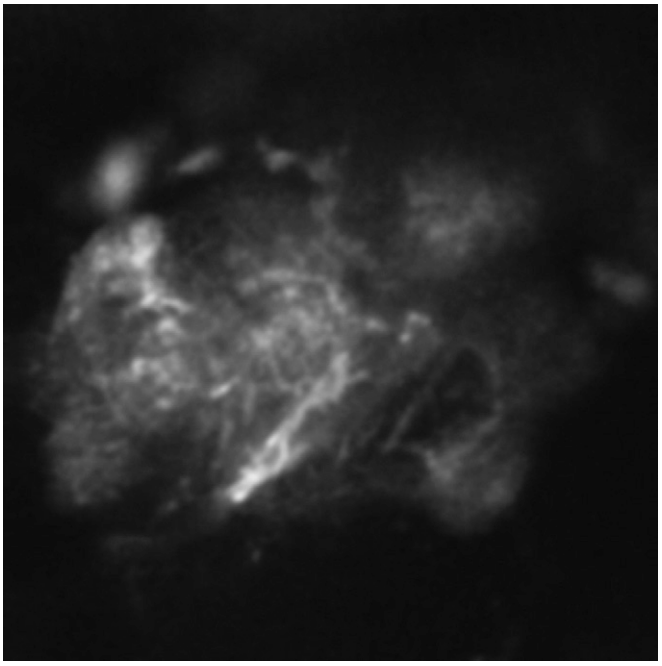

Movie S3. Z stack of right antennal lobe of anesthetized *GH146-Gal4,UAS-GCaMP3* fly. Each of the 127 slices in the image stack is an average of eight 512 × 512 pixel frames acquired with a 2.8-μs pixel dwell time. The field of view is 92 μm in both dimensions. The axial increment between slices was 1 μm. Laser illumination was 920 nm in wavelength and 10 mW of power at the specimen plane. The anesthesia removed almost all of the residual brain movement and thereby allowed us to acquire crisp images of baseline fluorescence. Based on our prior experience imaging manually dissected flies (1), we did not observe any laser-induced damage to the glomeruli or to the axons projecting to the mushroom body or lateral horn.

1. Liang L, et al. (2013) GABAergic projection neurons route selective olfactory inputs to specific higher-order neurons. *Neuron* 79(5):917–931.

Movie S3